A spatio-temporal mathematical model for the dynamics of paclitaxel in cell monolayers.

Isaac Proudfoot
Giulia Vallardi
Yoko Shishikura
Ola Epemolu
Mariya Ptashnyk
Adrian T. Saurin
Philip J. Murray

Abstract

Paclitaxel is a major chemotherapeutic drug used to treat a variety of tumour types. Through targeting microtubules, paclitaxel induces abnormal or arrested cell mitosis, leading to tumour shrinkage. The cytotoxicity of paclitaxel limits its clinical use, it is effective only at treating certain tumour types and it is not possible to predict which patients will respond well to treatment. The newer anti-mitotic drugs that have been developed to overcome some of these problems have thus far been less effective than paclitaxel in the clinic. One property of paclitaxel that distinguishes it from many of these other anti-mitotic drugs is its ability to concentrate within cells, a property that could allow intra-tumour concentrations to remain higher for longer following drug dosing. In this paper we seek to develop a mathematical model that can explain observations of paclitaxel uptake in isolated monolayer cultures. We perform a series of experiments on HeLa cell monolayers in which intracellular paclitaxel concentrations are measured under different treatment protocols. We then derive a spatially homogeneous model of paclitaxel uptake and use Bayesian inference to identify model parameters. As a prediction from this model was found to be inconsistent with a further set of experimental results, we consider a generalisation of the model to account for spatio-temporal dynamics and resolve the disparity between theory and experiment. The subsequent inclusion of the spatio-temporal dynamics provides a theoretical framework for the model to be extended to explain drug retention within multilayered tissues. This is important because paclitaxel penetration and release is expected to depend on local 3D tissue architecture.

Keywords: paclitaxel, mathematical models, microtubules, cancer modelling

1 Introduction

Cancer is driven by a huge variety of complex and diverse genetic alterations that converge onto just a few common phenotypic traits. These "hallmarks of cancer" allow tumour cells to proliferate at an abnormal rate and potentially migrate at the expense of healthy cells and tissues in the body [1]. It is estimated that one out of every two persons born today in the UK will develop cancer in their lifetime [2].

If the location of the cancer is unknown or uncertain, chemotherapy is often the most effective treatment option. This involves administering pharmaceutical compounds that can selectively kill tumour cells. Selectivity can be achieved by aiming for features that distinguish the tumour cells from healthy cells within the body. These can be either genetic or phenotypic differences, and currently the vast majority of chemotherapies specifically target rapidly dividing cells, a common feature of almost all tumour types. However, a major problem in this regard is that subpopulations of healthy cells in the body (e.g. in the blood, gut and skin) also proliferate rapidly and are therefore particularly susceptible to chemotherapeutic killing. As well as making patients extremely ill, these off-target effects result in severe dose-limiting toxicities that limit treatment effectiveness [3].

Paclitaxel (taxol) was identified in 1971 to be the cause of cytotoxicity of Pacific Yew tree bark [4]. It was one the first "blockbuster" oncology drugs and remains one of the most effective chemotherapeutic agents in widespread clinical use today [5, 6]. Paclitaxel is known to stabilise microtubule fibres and disrupt the mitotic spindle [7], resulting in either mitotic arrest or abnormal separation of the duplicated chromosomes; two fates that can ultimately lead to either cell death or permanent cell cycle arrest (senescence) [8, 9]. Whilst paclitaxel is effective at treating a range of tumour types (e.g. breast, ovarian, prostate, lung) [10, 11, 12, 13], it is also incredibly toxic to patients. Some of these toxicities, such as neutropenia, are life-threatening and require the dose and duration of treatment to be restricted [14]. Furthermore, neuronal side effects, which result from the stabilisation of microtubules in neurons, are also common [15], an effect that is unrelated to the desired effects on mitosis.

The cytotoxic side effects of paclitaxel have prompted many pharmaceutical companies to develop second-generation, mitosis-targeting drugs that could eventually replace paclitaxel and/or offer additional treatment options for the many patients that, for some unknown reason, do not respond well to paclitaxel treatment [16]. Whilst anti-mitotic drugs that act specifically to inhibit different aspects of cell division (e.g. microtubule motors and mitotic kinases) have been shown to effectively restrict tumour growth in animal models, these drugs have so far failed to offer the same benefits as paclitaxel when tested in clinical trials against various tumour types [17, 18]. These disappointing results reinforce the need to identify the properties of paclitaxel that underpin its clinical efficacy, which may also help us to understand why some patients or tumour types respond better to treatment than others [19].

A major difference between paclitaxel and the newer anti-mitotic drugs is

that paclitaxel has unique pharmacodynamics: when applied in cell culture it concentrates inside the cell and is released relatively slowly upon media washout [8, 20]. It is thought that the ability to become "trapped" inside cells could allow paclitaxel to persist within tumours for a long time after blood levels of the drug have declined. This could explain why paclitaxel can be retained in tumour for over a week after the blood levels have fallen [21]. Furthermore, this property may be particularly important in human disease when the rate of tumour proliferation is typically much slower than in animal models.

The molecular interactions of paclitaxel have previously been characterised. Paclitaxel molecules diffuse freely across the cell membrane. This was deduced by treating cells with sodium azide, which depletes ATP, which was found not to reduce the intracellular accumulation of paclitaxel [22]. Paclitaxel binds to a site on the $\beta-$tubulin subunit of polymerised tubulin dimers [23]. Thus the binding of paclitaxel to microtubules is saturable, with the limit of bound paclitaxel being the concentration of polymerised tubulin in the cell (i.e. up to $30\mu M$) [22, 24]. Additionally, a non-specific, non saturable binding also occurs [25, 22]. At high concentrations, paclitaxel has been shown to both rapidly induce tubulin polymerisation and increase the total amount of tubulin [25, 24].

A mathematical model for paclitaxel dynamics, composed of a system of ordinary differential equations, has previously been developed and fitted to experimental measurements from MCF7 cells [25]. The model accounts for paclitaxel concentrations in different intracellular and extracellular compartments and accounts for the high intracellular concentrations that are observed experimentally. In particular, this model indicates that there is a nonlinear relationship between the initial paclitaxel concentration in media and the intracellular paclitaxel concentration.

In this study we consider an experimental system in which monolayers of HeLa cells are exposed to a variety of paclitaxel treatment protocols. We use mass spectrometry to measure the total intracellular paclitaxel concentration as a function of a variety of experimentally controlled variables. We derive a spatio-temporal model that describes the key known features of paclitaxel kinetics and use it to provide a theoretical framework to interpret the experimental observations. The layout of the paper is as follows: in Section 2 we develop the model and describe the experimental set up; in Section 3 we describe the experimental results and fit the mathematical models to the experimental data; and, finally, in Section 4 we conclude with a discussion.

2 Methods

2.1 Sample preparation, paclitaxel measurement and experimental protocols

HeLa cells from ATCC were authenticated by STR profiling (Eurofins) and cultured in DMEM supplemented with 9% FBS, 50 μg/mL penicillin/streptomycin and 2 mM L-glutamine. All cell lines were routinely screened (every 4 - 8

Figure 1: Schematic illustration of the experimental protocols. (a) Protocol 1: Cells are treated paclitaxel media for 24 hours. (b) Protocol 2: Cells are treated paclitaxel media for 2 hours. The media is then washed out and replaced with drug free medium and left for a further 24 hours.

weeks) to ensure they were free from mycoplasma contamination. Paclitaxel was purchased from Selleckbio. Various dilutions ranging from 1 to 5000nM were prepared in media.

For sample collection, HeLa cells were plated in 6-well plates to reach near confluence at the time of the experiments. The free intracellular concentration was determined when required, using a method developed by *Mateus et al* [26]. To harvest cells for measurement of intracellular paclitaxel concentrations, cells were rapidly washed three times with ice-cold PBS (to fully remove extracellular paclitaxel) prior to lysis in a lysate buffer (composition: 20mM Tris, 150mM, NaCl, 1% Triton x100 and 1 pill per 10ml of proteases inhibitor- Sigma). After lysis, the lysed cells (lysate) were re-suspended in 2ml of ice cold PBS. 100μL of re-suspended lysate was then subjected to solvent crash in a 1:2 ratio of lysate to acetonitrile containing internal standard-5ng/ml of Donepezil. The concentration was determined with the aid of an appropriate calibration curve and UPLC-MS/MS. The unbound intracellular compound concentration (free fraction) was determined by dialyzing 150μL of re-suspended cell lysate against isotonic phosphate buffer in an equilibrium dialysis equipment. This was also subjected to UPLC-MS/MS.

In Protocol 1 HeLa cells were cultured for 24 hours in 6-well plates with 2 ml media containing a given concentration of paclitaxel (see Figure 1a). At various timepoints throughout this incubation, cells were lysed to measure intracellular paclitaxel concentrations. A series of follow up experiments was performed in which the total volume of the culture medium was varied (2 ml , 1 ml and 10 ml). Additionally, an identical procedure to this was conducted without cells, with the total concentration of paclitaxel in the medium measured at various timepoints.

In Protocol 2 HeLa cells were cultured for 2 hours in 6-well plates with 2 ml media containing 100 nM paclitaxel (see Figure 1b). Thereafter, media was washed out and replaced by fresh media (without paclitaxel). Cells were then cultured for different time periods over the course of 24 hours before harvesting

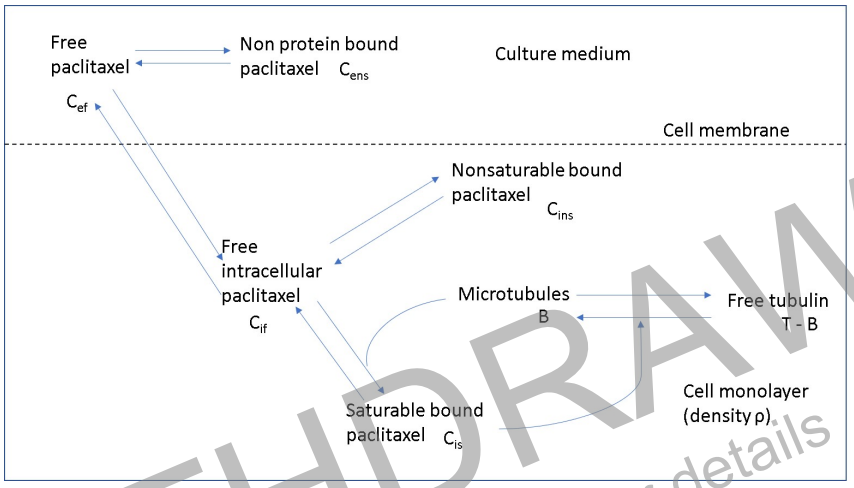

Figure 2: A schematic diagram illustrating the kinetics of paclitaxel in a single cell.

and intracellular paclitaxel concentration was measured.

2.2 Model Development

2.2.1 The ODE model

To develop a mathematical model of paclitaxel uptake, we make the following assumptions (see Figure 2): (i) paclitaxel concentrations are spatially homogeneous; (ii) free paclitaxel is transported across the cell membrane via passive diffusion [25, 22]; (iii) saturable paclitaxel binding to microtubules follows mass action kinetics; (iv) microtubule-bound paclitaxel promotes the further polymerisation of tubulin dimers and the production of new tubulin [25, 24]; and (v) the total number of molecules of paclitaxel in the system is conserved [25].

We define the following dependent variables: $C_{if}(t)$ represents the free intracellular concentration of paclitaxel; $C_{is}(t)$ represents the concentration of microtubule bound intracellular paclitaxel; $C_{ins}(t)$ represents the nonsaturable bound intracellular paclitaxel; $C_{ef}(t)$ represents the free extracellular concentration of paclitaxel; $C_{ens}(t)$ represents the concentration of paclitaxel that is bound to non-protein components in the extracellular domain; $T(t)$ represents the total concentration of tubulin in the cell; and $B(t)$ represents the concentration of microtubules in the cells.

After applying the above assumptions, a system of ODEs that describe the rate of change of each of the variables is derived and nondimensionalised (see Appendix A.1). To simplify the model, it is additionally assumed that C_{is} and C_{ins} are in pseudo-equilibrium. Hence we obtain a nondimensionalised system

of five ODEs and two algebraic equations given by

$$\begin{aligned}
\frac{dC_{if}}{dt} &= \lambda_1(C_{ef} - C_{if})\,,\\
C_{is} &= \frac{BC_{if}}{\frac{1}{\lambda_2} + C_{if}}\,,\\
C_{ins} &= \lambda_3 C_{if}\,,\\
\frac{dC_{ef}}{dt} &= \lambda_1 N_0 \frac{V_{onecell}}{V_{medium}}(C_{if} - C_{ef}) - \lambda_4 C_{ef} + \lambda_5 C_{ens}\\
\frac{dC_{ens}}{dt} &= \lambda_4 C_{ef} - \lambda_5 C_{ens}\,,\\
\frac{dT}{dt} &= \lambda_6 - \lambda_7(T - B)\,,\\
\frac{dB}{dt} &= (\lambda_8 + \lambda_9 C_{is})(T - B) - 2\lambda_8 B\,,
\end{aligned} \tag{1}$$

where λ_i, for $i = 1\,, ..., 9\,$, are constant model parameters. The initial conditions are given by

$$\begin{aligned}
&C_{if}(0) = C_{is}(0) = C_{ins}(0) = 0, \quad C_{ef}(0) = C_0,\\
&C_{ens}(0) = 0, \quad T(0) = \frac{T_0}{B_0}\,, \quad B(0) = 1\,,
\end{aligned} \tag{2}$$

represent the case in which cells are treated with paclitaxel. We also define the dimensional total intracellular concentration to be

$$C(t) = \bar{K}C_{if}(t) + T_0 C_{is}(t) + \bar{K}C_{ins}(t)\,, \tag{3}$$

where $\bar{K} = 1\mu M$ and $T_0 = 18.9\mu M$ (see Table 5 for further details on these scalings). It should be noted that when comparing the fit of equations (1), (2) with the experimental data, the dimensional total intracellular concentration will always be used.

2.2.2 The PDE model

To account for the cells being contained in a monolayer at the bottom of a well in the experimental setup, we consider the case of a cylindrical dish of radius R that contains a monolayer of cells of density ρ and thickness d that is positioned at the bottom of the dish ($z = 0$). We let $h_i\,, i \in \{1, 2, 3\}$ represent the height of the extracellular fluid depending on the volume of medium used in the experimental protocol (see Appendix A.3 for details on the specific values), and Z_0 represent the maximum height of the fluid used across all the experimental protocols. Both free and bound extracellular paclitaxel are assumed to diffuse through the medium with diffusion coefficient, D. Retaining the kinetic assumptions from Section 2.2.1, a spatial model is derived and nondimensionalised (see Appendix (A.2)). We apply the same simplifications as for the ODE model together with the assumption that the density of cells in the monolayer

ρ is constant and that the solution is axisymmetric. In the cellular domain ($0 < z < \delta_1$, where $\delta_1 = \frac{d}{Z_0}$) we obtain a coupled system of reaction-diffusion, partial differential and algebraic equations given by

$$\begin{aligned}
\frac{\partial C_{if}}{\partial t} &= \tilde{\lambda}_1(C_{ef} - C_{if})\,,\\
C_{ins} &= \lambda_3 C_{if}\,,\\
C_{is} &= \frac{BC_{if}}{\frac{1}{\lambda_2} + C_{if}}\,,\\
\frac{\partial C_{ef}}{\partial t} &= \bar{D}\frac{\partial^2 C_{ef}}{\partial z^2} + \lambda_1\frac{(1-\rho)}{\rho}(C_{if} - C_{ef}) - \lambda_4 C_{ef} + \lambda_5 C_{ens}\,,\\
\frac{\partial C_{ens}}{\partial t} &= \lambda_4 C_{ef} - \lambda_5 C_{ens}\,,\\
\frac{\partial T}{\partial t} &= \lambda_6 - \lambda_7(T - B)\,,\\
\frac{\partial B}{\partial t} &= (\lambda_8 + \lambda_9 C_{is})\,(T - B) - 2\lambda_8 B\,.
\end{aligned} \tag{4}$$

In the extracellular domain ($\delta_1 < z < \delta_2$, where $\delta_2 = \frac{h_i}{Z_0}$,) the governing equations are given by

$$\begin{aligned}
\frac{\partial C_{ef}}{\partial t} &= \bar{D}\frac{\partial^2 C_{ef}}{\partial z^2} - \lambda_4 C_{ef} + \lambda_5 C_{ens}\,,\\
\frac{\partial C_{ens}}{\partial t} &= \lambda_4 C_{ef} - \lambda_5 C_{ens}\,.
\end{aligned} \tag{5}$$

The initial conditions in the cellular domain ($0 < z < \delta_1$) are given by

$$\begin{aligned}
&C_{if}(z,0) = C_{is}(z,0) = C_{ins}(z,0) = 0\,,\ C_{ef}(z,0) = C_0\,,\\
&C_{ens}(z,0) = 0\,,\ T(z,0) = 1\,,\ B(z,0) = \tilde{B}\,.
\end{aligned}$$

The initial conditions in the extracellular domain ($\delta_1 < z < \delta_2$) are given by

$$C_{ef}(z,0) = C_0\,,\ C_{ens}(z,0) = 0\,.$$

The system is closed with the following zero-flux boundary conditions

$$\left.\frac{\partial C_{ef}}{\partial z}\right|_{(0,t)} = 0, \quad \left.\frac{\partial C_{ens}}{\partial z}\right|_{(0,t)} = 0, \quad \left.\frac{\partial C_{ef}}{\partial z}\right|_{(\delta_2,t)} = 0, \quad \left.\frac{\partial C_{ens}}{\partial z}\right|_{(\delta_2,t)} = 0. \tag{6}$$

For this model we define the dimensional total intracellular concentration to be the average of the sum of the rescaled intracellular concentrations across the cellular region

$$C(t) = \frac{1}{\delta_1}\int_0^{\delta_1} (\bar{K}C_{if}(z,t) + T_0 C_{is}(z,t) + \bar{K}C_{ins}(z,t))dz\,. \tag{7}$$

2.3 Numerical solution

Equations (1), (2) were solved using *MATLAB's* built in ode15s solver [27]. The method of lines was used to calculate numerical solutions of equations (4) – (6), with corresponding initial and boundary conditions.

The spatial domain was discretised using a logarithmic scaled as the concentration gradients near $z = 0$ are much larger than elsewhere. The discretisation is given by the following formula:

$$\begin{aligned} z_0 &= 0\,, \\ z_i &= \delta_1 \left(10^{\frac{i}{M_1-1}-1}\right)\,, \qquad i = 1, ..., M_1 - 1\,, \\ z_i &= \delta_1 + (\delta_2 - \delta_1)\left(10^{\frac{i-M_1}{M_p-1-M_1}-1}\right)\,, \quad i = M_1, ..., M_p - 1\,, \end{aligned} \tag{8}$$

where M_1 represents the total number of discretisation points of the cellular domain, and M_p represents the total number of discretisation points. Spatial derivatives were approximated using a finite difference approximation. The ode15s solver was used to solve the resultant system of coupled ODEs.

2.4 Parameter inference

Model parameters were estimated using a Bayesian framework. The parameters λ_6, λ_7, λ_8, D were fixed with reference to the literature (see Table 4). The parameters λ_1, λ_2, λ_3, λ_4, λ_5, λ_9 are represented by the vector Θ and determined as described below.

We assumed non-informative priors for each of the unknown parameters, i.e.

$$\Theta_j \in U_{[a_{lj}, b_{uj}]}, \quad j = 1, .., 6\,, \tag{9}$$

where $U_{[a_{lj}, b_{uj}]}$ represents a uniform distribution with lower and upper bounds a_j and b_j, respectively (see Table 3 for the particular values).

The likelihood for the j^{th} data point in the i^{th} experiment, L_{ij}, was given by assuming a normal error distribution, i.e.

$$L_{ij} \propto e^{-\left(\frac{\Delta E_{ij}}{\sigma_{ij}}\right)^2}\,, \tag{10}$$

where

$$\Delta E_{ij} = Q_{ij} - C(t_j)\,. \tag{11}$$

Q_{ij} is the measured total intracellular paclitaxel at the j^{th} time point t_j, in the i^{th} experiment. $C(t_j)$ represents the corresponding rescaled total intracellular paclitaxel given by the numerical simulation of the model at t_j. When considering the ODE model given by equations (1), (2), $C(t_j)$ is given by (3); and for the PDE model given by (4) – (6), C_{t_j} is given by (7). We define

$$\sigma_{ij} = Q_{ij} - \mu_i \tag{12}$$

where μ_i represents the mean intracellular paclitaxel measurement in a given experiment. Hence, the total likelihood is given by

$$L(\Theta) \propto \prod_{i=1}^{n} \prod_{j=1}^{N_i} e^{-\left(\frac{\Delta E_{ij}}{\sigma_{ij}}\right)^2}. \tag{13}$$

where n represents the total number of experiments and N_i represents the number of measurements in the i^{th} experiment. The log-likelihood, $l(\Theta)$, is given by

$$l(\Theta) = \ln(L(\Theta)) \propto \sum_{i=1}^{n} \sum_{j=1}^{N_i} -\left(\frac{\Delta E_{ij}}{\sigma_{ij}}\right)^2.$$

The posterior distribution is therefore given by

$$f(\Theta) \propto \left(\prod_{k=1}^{m_k} \frac{1}{b_{uk} - a_{lk}}\right) L(\Theta), \tag{14}$$

where m_k is the number of parameters being optimised over.

A Gibbs sampler with a Metropolis-like acceptance criterion was used to estimate the posterior distribution. Let Θ_i^{k+1} be the parameter vector with the i^{th} parameter sampled for the $k+1$st time, then the probability of accepting Θ_i^{k+1} in the Metropolis-Hastings algorithm is given by

$$\mathbb{P}\left(\text{Accept } \Theta_i^{k+1}\right) = \min\left(1\,, \frac{f(\Theta_i^{k+1})}{f(\Theta_{i-1}^{k+1})}\right). \tag{15}$$

For numerical stability, the logarithm of the ratio of the old and new marginal density functions is used, where

$$\begin{aligned} \mathbb{P}\left(\text{Accept } \Theta_i^{k+1}\right) &= \min\left(1\,, \ln\left[\frac{f(\Theta_i^{k+1})}{f(\Theta_{i-1}^{k+1})}\right]\right), \\ &= \min\left(1\,, l(\Theta_i^{k+1}) - l(\Theta_{i-1}^{k+1})\right), \end{aligned} \tag{16}$$

The Gibbs sampler is run for a total of Ψ iterations, with a burn in period of Ψ_b to ensure that the sampler has converged to a stationary distribution (see Table 2).

3 Results

3.1 A spatially homogeneous model

To quantify background paclitaxel dynamics in the absence of cells, we measured the paclitaxel concentration in the media as a function of time. We observed that the paclitaxel concentration is a decreasing function of time (see Figure 3(b)).

Figure 3: (a) A schematic illustration of the model. (b) Total extracellular paclitaxel concentration is plotted against time. Black line - rescaled numerical solution of $C_{ef} + C_{ens}$ from system (28). Red crosses - measured free paclitaxel concentration in extracellular media. Parameters values defined in Table 4. (c) Scatter plot of the accepted values of the extracellular parameters λ_4 and λ_5 when sampled from the uniform prior. Black dotted lines indicate values of sample medians.

As the half life for paclitaxel degradation in aqueous solution is known to be greater than 24 hours [25], we assume that paclitaxel loss from the extracellular media is due to binding to some other component in the system (e.g. the container walls).

We developed a mathematical model that is a subsystem of equations (1), (2), in which free paclitaxel can reversibly transfer to a nondetectable pool (see Figure 3 (a) and Appendix B.1). To infer the optimal parameter values (see Table 4), we applied Bayesian inference with uniform priors and estimated posterior distributions for the parameters λ_4 and λ_5 (see Method 2.4). Local maxima were identified for the marginal posterior distributions (see Figure 6 for further details). The equations (1), (2) provide an excellent fit to the available experimental data.

To quantify the cellular uptake of paclitaxel by HeLa cells, a set of experiments was performed in which monolayers of HeLa cells were cultured in 6 well plates and intracellular paclitaxel was measured under different treatment protocols. We found that (Protocol 1) cellular uptake of paclitaxel occurred on a timescale of minutes and that intracellular concentrations reached micromolar concentrations within an hour (see Figure 4 (a)). We also identified that the intracellular paclitaxel concentration observed after two hours of incubation shows a strong nonlinear dependence on initial paclitaxel concentration (see Figures 4(b) and 4(c)). These experimental results are consistent with previous measurements by [25] on MCF7 cells. We performed washout experiments in which media was replaced after two hours (Protocol 2) and found that the intracellular paclitaxel concentration decreases rapidly to a steady state that is approximately half the concentration at the point of washout (see Figures 4(b) and 4(c)).

To account for the measurements of paclitaxel uptake by HeLa cells, we

developed an ordinary differential equation model (see Section 2.2.1), that describes binding of paclitaxel to microtubules, non-specific intracellular binding, flux of paclitaxel across the cell membrane and the extracellular loss term measured in Figure 3. To identify the parameter values that best-fitted the experimental measurements in Figure 4(a)-(c), we employed Bayesian inference. We identified unique maxima for the posterior distributions (see Appendix B). In Figures 4(a)-(c) we plot the model solution using the median of the sampled parameter values. Note that the model captures the two timescales of intracellular paclitaxel dynamics that are observed in the experimental data.

A testable prediction of the mathematical model is that the intracellular paclitaxel concentration increases with the volume of extracellular media. To test this hypothesis, we performed a series of experiments at different media volumes (1 ml, 2 ml and 10 ml). We found that intracellular paclitaxel concentrations did increase with media volume but that the magnitude of the increase was underestimated by the model (see Figure 4(d)).

3.2 A spatio-temporal model

To address the deviation between model prediction and experimental measurements at large media volumes, we generalised the model to account for the diffusion of paclitaxel in extracellular media (see equations (4)-(6)). Notably, this introduced one parameter, the diffusion coefficient of paclitaxel in acqueous solution, whose value we taken from experimental measurements in the literature [28].

We numerically solved the PDE model (4)-(6) (see Section 2.3), and again employed Bayesian inference to infer the model parameters using the experimental presented in Figure 4(a)-(c). We assumed uniform priors for the unknown parameters and the posterior distributions were computed using a Gibbs sampling algorithm (see Section 2.4). We identified that the marginal posteriors were unimodal (see Figure 7), and using the 'best-fit' parameter plotted the fitted model solutions (see Figure 5(a)-(c)). Note that the parameters describing the relative binding kinetics to the various cellular components are almost exactly the same as in the case of the ODE model (1), (2). However, the value of α, which describes the rate of transport across the cell membrane, is a factor of 4 greater than the corresponding value obtained for the ODE model.

To test whether the PDE model could predict the experimental observations of intracellular paclitaxel concentrations in different volumes of media, we computed the numerical solution of equations (4)-(6) at different media volumes by varying the boundary condition. Remarkably, the model provides an excellent prediction of the measured intracellular concentration of paclitaxel after 2 hours (see Figure 5(d)). These results suggest that spatio-temporal effects ought to be accounted for in the case of moderately larger volumes.

Figure 4: A comparison of the fit of the spatially homogeneous model (1), (2) to experimental measurements. (a) Total intracellular paclitaxel concentration, $C(t)$, is plotted against time for an initial concentration of $C_{initial} = 100nm$. Control media (circles - experimental data, solid line - model solution). (b) Total intracellular paclitaxel concentration, $C(t)$, is plotted against the initial paclitaxel concentration, $C_{initial}$, after a two hour paclitaxel incubation (crosses - experimental data, solid black line - model solution) followed by eight hours in control media (red and blue circles- experimental data, dotted black line - model solution). (c) Total intracellular paclitaxel concentration, $C(t)$, is plotted against time after 2 hours of incubation of cells in 100nM of paclitaxel (red markers - data, red curve - model with fitted parameters). (d) Total intracellular paclitaxel concentration after a two hour incubation, $C(2)$ is plotted against the dimensional initial concentration, $C_{initial}$, for different media volumes (1 ml - red, 2 ml - blue and 10 ml -black) (lines - model solutions, crosses - experimental data). The model was solved using the Method defined in Section 2.3. For the parameter values see Table 4.

Figure 5: A comparison of the fit of the PDE model (4)-(6) to experimental measurements. (a) Total averaged over spacial domain intracellular paclitaxel concentration, $C(t)$, is plotted against time with an initial concnetration of $C_{initial} = 100nM$. Control media - experimental data (circles) and model (solid line). (b) Total averaged over spacial domain intracellular paclitaxel concentration, $C(t)$, is plotted against initial paclitaxel concentration, $C_{initial}$, after a two hour paclitaxel incubation (crosses - experimental data, solid black line - model solution) followed by eight hours in control media (red and blue circles - experimental data, dotted black line - model solution). (c) Total averaged over spacial domain intracellular paclitaxel concentration, $C(t)$, is plotted against time after 2 hours of incubation of cells in 100nM of paclitaxel (red markers - washout in control media, red curve - fitted model). (d) Total averaged over spacial domain intracellular paclitaxel concentration after a two hour incubation, $C(2)$, is plotted against initial concentration, $C_{initial}$, for different media volumes (1 ml - red, 2 ml - blue and 10 ml -black) (lines - model solutions, markers - experimental data). The model was solved using the method defined in Section 2.3. For parameter values see Table 4.

4 Discussion

Paclitaxel is one of the most important broad-spectrum chemotherapeutic drugs in clinical use today. It's main known mechanism of action is to inhibit mitosis via interference with microtubule dynamics. As paclitaxel dosing is limited by side effects, billions of pounds have been spent to develop next-generation anti-mitotic drugs that target specific features of mitosis (e.g. PKA, Aurora Kinase inhibitors). Whilst many of the next-generation drugs have shown efficacy in mouse models, they have thus far proved to be less effective than paclitaxel in clinical trials [17, 18]. These data reinforce the need to understand precisely what features of paclitaxel allow it perform better then these newer generation drugs.

In this paper we combined experimental and theoretical approaches in order to develop a data-driven model of paclitaxel uptake in HeLa cell monolayer cultures. We measured intracellular paclitaxel concentration in a background of different paclitaxel treatment protocols and identified nonlinearities in the data that motivate the need for theoretical approaches. We then developed mathematical models that enabled consistent interpretation of the experimental data and generated predictions that were tested experimentally.

We firstly developed an ordinary differential equation model that accounts for paclitaxel transport across the cell membrane, saturable binding to microtubules and non-saturable binding to other intracellular compartments. After simplifying the model, we employed Bayesian inference to infer the model parameter values and showed that the model provides a good fit to the available experimental data. In order to test a prediction of the model, we varied the media volume and measured intracellular paclitaxel concentration. Intriguingly, we found that the model was unable to quantitatively predict the outcome of the volume change experiment.

Motivated by the fact that there is a strong sink of paclitaxel on one boundary and that such an asymmetry could lead to significant spatial gradients along the azimuthal axis of the well, we generalised the model to account for diffusion of paclitaxel in the extracellular space. We used Bayesian inference to infer model parameters using experimental measurements made at 2 ml media. The model solution with 'best-fit' parameters provided an excellent agreement with the experimental observations. Moreover, upon comparing parameter values with the ODE solution we noted that although most of the parameters remained unchanged, a notable exception was the parameter α, which represents the rate at which paclitaxel crosses the cell membrane, was four fold larger for the PDE model. Remarkably, when we tested the prediction of the PDE model using different media volumes volumes we found excellent agreement with the experimental observations. These results demonstrate that the volume of the media has a significant effect on paclitaxel uptake kinetics. The number of cells is also a critical factor, and yet neither of these parameters were reported in a recent major study examining the concentrating effect of paclitaxel in cell lines and patient tumours [9].

Whilst this study builds upon the previous work of Kuh et al. [25], we note

that there are a number of major differences between approaches: Kuh et al. accounted for the effect of intracellular paclitaxel on microtubule concentration by making a model parameter a function of initial paclitaxel concentration. However, we have accounted for this interaction via explicit variable dependence; we have developed a spatio-temporal model that is valid in the limit of large media volumes; we have provided a general model derivation for which the pseudo-steady approximation is a special case; and we have quantified uncertainty in parameter estimates using a Bayesian framework. With regard to experimental data, we have performed experiments on a different cell line (HeLa cells) and have conducted novel washout experiments.

When comparing parameters fitted for the ODE and PDE models respectively (see Tables 4 and 5), we find that a majority of the parameters are almost identical when both systems are fitted to the same data, with the exception of the parameter α, the clearance of the drug from diffusion across the cell membrane. When the values for λ_1 and $\tilde{\lambda}_1$ are converted back to the clearance coefficient α, we find, upon taking the average of the PDE system (4) – (6) over the spatial domain (see Supplementary Material), that the two clearance coefficients for the cell membrane are different by approximately a factor of 4. However, when the concentration profiles over time of the two models are compared, we see that both the ODE and PDE models attain the same steady state (within numerical error), and that the two profiles are similar at 1 ml (see Figure 8 for details). Hence, this large change in the interpreted value of α is due to the difference between the dynamics immediately following the introduction or removal of paclitaxel from the medium in the different cases. This indicates that estimates of this parameter may prove unreliable if an assumption of spatial homogeneity is made.

Song et al. have previously studied paclitaxel kinetics in a range of experimental conditions. They measured that the decrease in extracellular paclitaxel concentration occurs on two distinct time scales, an initial transient followed by a slow reduction. In the presence of FBS the reduction in measurable paclitaxel concentration is no longer present. However, they did measure binding of paclitaxel to extracellular protein in the presence of FBS. In contrast, in our experimental measurements (see Figure 3), we identify a decrease in paclitaxel concentration in the presence of FBS. To ensure the main conclusions from this manuscript are robust to the inclusion of these details, we have formulated alternative models in which we account for: (i) binding of extracellular paclitaxel to media proteins; (ii) linear degradation of paclitaxel in extracellular space (see Appendix D). In all considered cases the main results of the manuscript are unchanged.

Whilst the PDE approach is able to predict the effect of media volume changes, we have also explored the difference between ODE and PDE models across a range of variables available to the experimentalist (initial paclitaxel concentration, time of measurement of intracellular paclitaxel and media volume). We find that in the limit of large times (say 24 h) the solutions of the ODE and PDE models converge to the same steady state. The maximum difference between the modelling frameworks occurs at small times, large initial

concentrations and large volumes (see Appendix C). However, one major advantage of the PDE framework is that it naturally extends to multi-cell layered tissue.

Paclitaxel has been shown to kill cancer cells by perturbing cell mitosis through microtubule stabilisation [9, 8]. However, many chemosensitive tumours have a low overall proliferation rate, making this claim controversial [18, 29]. Additional benefits of paclitaxel identified to potentially resolve this 'proliferation rate paradox', as described by *Mitchsion*, are drug retention, effects on microtubules that are unrelated to mitosis, or bystander killing from other cell types such as immune cells [30]. Recently, immune cell killing was proposed to be induced by the post-mitotic micronucleation observed following clinically relevant drug doses [31, 9]. It is important to determine the relative contribution of these different features to tumour shrinkage following paclitaxel treatment.

However, irrespective of the final mechanism(s) of action, it is critical to understand how paclitaxel is taken up and retained within tumour tissue. To help model and predict this non-linear behaviour, we have measured paclitaxel uptake in cell monolayers and developed, validated and tested a mathematical model. This has allowed us to quantify the retention of paclitaxel in a monolayer. The next step for this work is to generalise the model so that it can be applied to the study of paclitaxel uptake in three dimensional spheroids, with the ultimate goal of using a data-driven modelling approach to study of tumour growth *in vivo*. This may eventually help us to better understand why paclitaxel treatment works only in a subset of tumours and patients, and why it remains a more effective clinical compound than many of the new generation anti-mitotic drugs.

5 Acknowledgments

ATS is funded by a Cancer Research UK PFA award (C47320/A21229 to ATS) and GV was funded by Tenovus Scotland.

A Model Formulation

A.1 The ODE Model

Binding kinetics It is also assumed that paclitaxel binds to some nonprotein component in the extracellular domain following mass action kinetics. The forward and reverse binding rates are given by k_5 and k_6 respectively. We assume that free paclitaxel binds saturably to microtubules following mass action kinetics, thus the forward binding is given by $k_1(B - C_{is})C_{if}$, where k_1 is the rate constant. The rate of dissociation of paclitaxel from the microtubules is assumed to be linear with rate constant k_2. Additionally, paclitaxel is assumed to bind without saturation to various other cellular components following mass action kinetics. The forward binding rate constant is given by k_3 and the dissociation rate constant is k_4.

Transport across cell membrane It is assumed that free paclitaxel is transported across the cell membrane by passive diffusion [25], with the diffusion limited by the permittivity of the cell membrane α. The total number of molecules of paclitaxel inside the cells at time t is given by $C(t)$. The rate of transfer of paclitaxel across the cell membrane is given by $\alpha(C_{ef} - C_{if})$, where α is the permittivity of the cell membrane. In particular, to conserve the total number of molecules of paclitaxel in the system, the flux rate of paclitaxel into the cells is given by $\frac{\alpha}{V_{onecell}}(C_{ef} - C_{if})$, where $V_{onecell}$ is the volume of one cell. Since it is assumed that the cells are uniformly dispersed throughout the medium, the efflux rate of paclitaxel is given by $\frac{\alpha \cdot N}{V_{medium}}(C_{if} - C_{ef})$, where V_{medium} is the total volume of the medium used in the experiment, and N_0 is the total cell population, which is assumed constant.

Microtubule dynamics We assume that new α- and β-tubulin monomers are both transcribed at a rate a_1. It is also assumed that tubulin monomers decay at a rate a_3. The initial concentration of microtubules is taken to be $B_0 = 6.3\mu M$, with the total initial concentration of tubulin monomers assumed to be three times larger $T_0 = 18.9\mu M$ [24]. Furthermore, it is assumed that in the absence of paclitaxel, the stationary values of T and B are assumed to be T_0 and B_0 respectively, thus we set $a_1 = a_3(T_0 - B_0)$.

Then the spatially-homogeneous model for the pharmacokinetics of paclitaxel is given by

$$\begin{aligned}
\frac{dC_{if}}{dt} &= \frac{\alpha}{V_{onecell}}(C_{ef} - C_{if}) - k_1(B - C_{is})C_{if} + k_2 C_{is} - k_3 C_{if} \\
&\quad + k_4 C_{ins}\,, \\
\frac{dC_{is}}{dt} &= k_1(B - C_{is})C_{if} - k_2 C_{is}\,, \\
\frac{dC_{ins}}{dt} &= k_3 C_{if} - k_4 C_{ins}\,, \\
\frac{dC_{ef}}{dt} &= \frac{\alpha \cdot N_0}{V_{medium}}(C_{if} - C_{ef}) - k_5 C_{ef} + k_6 C_{ens}\,, \\
\frac{dC_{ens}}{dt} &= k_5 C_{ef} - k_6 C_{ens}\,, \\
\frac{dT}{dt} &= a_1 - a_3(T - B)\,, \\
\frac{dB}{dt} &= (\beta_1 + \beta_2 C_{is})\,(T - B) - \beta_4 B.
\end{aligned} \tag{17}$$

Initially, at $t = 0$, a concentration of C_{initital} is administered, all of which is in the form of free extracellular paclitaxel, with all other paclitaxel concentrations assumed to be zero. It is assumed that the cells start with the normal concentration of microtubules, B_0, and the normal total concentration of α - and β - tubulin dimers in the system, T_0. Hence, the initial conditions are given by:

$$C_{if} = C_{is} = C_{ins} = 0,\ C_{ef} = C_{initital},\ C_{ens} = 0,\ T = T_0,\ B = B_0\,.$$

To nondimensionalise the system, scalings are chosen to reduce the number of parameters in the equations and to make the variables of the same order of magnitude. Since at the steady state the free intra- and extracellular concentrations are equal, the same scaling $\bar{K}$ is chosen for both of them. This also reduces the number of parameters in the equations for C_{ef} and C_{ens}. It has been found from previous studies that the maximum microtubule bound concentration of paclitaxel approaches the concentration of polymerised tubulin in the cells, and since the microtubule concentration is bounded above by the total concentration of tubulin monomers, the scalings for C_{is}, B and T are chosen to be T_0. Thus the nondimensionalised variables, represented by hats, are defined by

$$C_{if} = \bar{K}\hat{C}_{if}\,,\ C_{is} = T_0\hat{C}_{is}\,,\ C_{ins} = \bar{K}\hat{C}_{ins}\,,\ C_{ef} = \bar{K}\hat{C}_{ef}\,,$$
$$C_{ens} = \bar{K}\hat{C}_{ens}\,,\ T = T_0\hat{T}\,,\ B = T_0\hat{B}\,,\ t = \tilde{t}\hat{t}\,.$$

Substituting these scalings into system (17) and nondimensionalizing, the following system of dimensionless equations is obtained:

$$\begin{aligned}
\frac{d\hat{C}_{if}}{d\hat{t}} &= \frac{\alpha\tilde{t}}{V_{onecell}}(\hat{C}_{ef} - \hat{C}_{if}) - k_1T_0\tilde{t}\left(\hat{B} - \hat{C}_{is}\right)\hat{C}_{if} + \frac{k_2T_0\tilde{t}}{\bar{K}}\hat{C}_{is} \\
&\quad - k_3\tilde{t}\hat{C}_{if} + k_4\tilde{t}\hat{C}_{ins}\,, \\
\frac{d\hat{C}_{is}}{d\hat{t}} &= k_1\bar{K}\tilde{t}(\hat{B} - \hat{C}_{is})\hat{C}_{if} - k_2\tilde{t}\hat{C}_{is}\,, \\
\frac{d\hat{C}_{ins}}{d\hat{t}} &= k_3\tilde{t}\hat{C}_{if} - k_4\tilde{t}\hat{C}_{ins}\,, \\
\frac{d\hat{C}_{ef}}{d\hat{t}} &= N_0\frac{\alpha\tilde{t}}{V_{medium}}(\hat{C}_{if} - \hat{C}_{ef}) - k_5\tilde{t}C_{ef} + k_6\tilde{t}C_{ens}\,, \\
\frac{d\hat{C}_{ens}}{d\hat{t}} &= k_5\tilde{t}\hat{C}_{ef} - k_6\tilde{t}\hat{C}_{ens} \\
\frac{d\hat{T}}{d\hat{t}} &= \frac{a_1\tilde{t}}{T_0} - a_3\tilde{t}(\hat{T} - \hat{B})\,, \\
\frac{d\hat{B}}{d\hat{t}} &= \left(\beta_1\tilde{t} + \beta_2\tilde{t}T_0\hat{C}_{is}\right)(\hat{T} - \hat{B}) - 2\beta_1\tilde{t}\hat{B}\,,
\end{aligned} \tag{18}$$

with the corresponding initial conditions:

$$\hat{C}_{if} = \hat{C}_{is} = \hat{C}_{ins} = 0\,,\ \hat{C}_{ef} = C_0\,,\ \hat{C}_{ens} = 0\,,\ \hat{T} = 1\,,\ \hat{B} = \tilde{B}\,.$$

Now define the following dimensionless parameters:

$$\lambda_1 = \frac{\alpha\tilde{t}}{V_{onecell}},\quad \lambda_2 = \frac{k_1\bar{K}}{k_2},\quad \lambda_3 = \frac{k_3}{k_4},\quad \lambda_4 = k_5\tilde{t},\quad \lambda_5 = k_6\tilde{t}, \tag{19}$$

$$\lambda_6 = \frac{a_1\tilde{t}}{T_0},\quad \lambda_7 = a_3\tilde{t},\quad \lambda_8 = \beta_1\tilde{t},\quad \lambda_9 = \beta_2T_0\tilde{t} \tag{20}$$

The dimensionless parameters $\lambda_i\,, i \in \mathbb{N}$ are given in terms of the full model parameters in the Grouping column of Table 4. Dropping hats, taking $\tilde{t} = 1$, and

applying the simplifications (vii)–(xii), described in Section 2.2.1, specifically the quasi-steady state assumptions on $\hat{C}_{is}$ and $\hat{C}_{ins}$; and substituting in the λ_i, we obtain model (1), (2).

A.2 The PDE Model

We apply the same assumptions on the binding kinetics and the effect on microtubules of paclitaxel as stated in assumptions (i)–(vi) from Section 2.2.1 (more details can be found in Appendix A.1), along with the assumption that extracellular paclitaxel diffuses through the medium with diffusion coefficient D defined in Section 2.2.2. In this case, the cells are assumed to be contained in a monolayer at the bottom of a cylindrical well ($0 < z \leq d$), distributed throughout this region with density ρ, which is assumed to remain constant. The rate of transfer of paclitaxel from the extracellular into the intracellular compartment in the monolayer is assumed to be given by $\alpha(1-\rho)(C_{ef} - C_{if})$, where α is the permittivity of the cell membrane. The transfer rate of paclitaxel from the intracellular compartment out into the medium is assumed to be given by $\alpha\rho(C_{if} - C_{ef})$. Hence, the full system of equations for the PDE model is given by:

For the region containing the monolayer of cells, ($0 < z \leq d$)

$$\begin{aligned}
\frac{\partial C_{if}}{\partial t} &= \alpha\rho(C_{ef} - C_{if}) - k_1(B - C_{is})C_{if} + k_2 C_{is} - k_3 C_{if} \\
&\quad + k_4 C_{ins}\,, \\
\frac{\partial C_{is}}{\partial t} &= k_1(B - C_{is})C_{if} - k_2 C_{is}\,, \\
\frac{\partial C_{ins}}{\partial t} &= k_3 C_{if} - k_4 C_{ins}\,, \\
\frac{\partial C_{ef}}{\partial t} &= D\frac{\partial^2 C_{ef}}{\partial z^2} + \alpha(1-\rho)(C_{if} - C_{ef}) - k_5 C_{ef} + k_6 C_{ens}, \\
\frac{\partial C_{ens}}{\partial t} &= k_5 C_{ef} - k_6 C_{ens}\,, \\
\frac{\partial T}{\partial t} &= a_1 - a_3(T - B)\,, \\
\frac{\partial B}{\partial t} &= (\beta_1 + \beta_2 C_{is})\,(T - B) - 2\beta_1 B\,,
\end{aligned} \tag{21}$$

and for the extracellular domain ($d < z < h$) we have

$$\begin{aligned}
\frac{\partial C_{ef}}{\partial t} &= D\frac{\partial^2 C_{ef}}{\partial z^2} - k_5 C_{ef} + k_6 C_{ens}\,, \\
\frac{\partial C_{ens}}{\partial t} &= k_5 C_{ef} - k_6 C_{ens}\,.
\end{aligned} \tag{22}$$

The initial conditions for the cellular domain ($0 < z \leq d$) are given by

$$\begin{aligned}
&C_{if}(z,0) = C_{is}(z,0) = C_{ins}(z,0) = 0\,,\ C_{ef}(z,0) = C_{\text{initital}}\,, \\
&C_{ens}(z,0) = 0\,,\ T(z,0) = T_0\,,\ B(z,0) = B_0\,,
\end{aligned}$$

and for the extracellular domain ($d < z < h$) the initial conditions are given by

$$C_{ef}(z,0) = C_{\text{initital}}\,, \quad C_{ens}(z,0) = 0\,.$$

The system is closed by the zero-flux boundary conditions

$$\left.\frac{\partial C_{ef}}{\partial z}\right|_{(0,t)} = 0, \quad \left.\frac{\partial C_{ens}}{\partial z}\right|_{(0,t)} = 0, \quad \left.\frac{\partial C_{ef}}{\partial z}\right|_{(h,t)} = 0, \quad \left.\frac{\partial C_{ens}}{\partial z}\right|_{(h,t)} = 0. \tag{23}$$

Substitute the scalings

$$\hat{C}_{if} = \bar{K}\hat{C}_{if}\,,\ \hat{C}_{is} = T_0\hat{C}_{is}\,,\ \hat{C}_{ins} = \bar{K}\hat{C}_{ins}\,,\ \hat{C}_{ef} = \bar{K}\hat{C}_{ef}\,,$$
$$\hat{C}_{ens} = \bar{K}\hat{C}_{ens}\,,\ \hat{T} = T_0\hat{T}\,,\ \hat{B} = T_0\hat{B}\,,\ \hat{t} = \tilde{t}\hat{t}\,,\ \hat{z} = L\hat{z}\,,$$

into (22) and nondimensionalize. Now define $\delta_1 = \frac{d}{Z_0}$, $\delta_2 = \frac{h_i}{Z_0}$. Then for $(0 < \hat{z} < \delta_1)$ we obtained

$$\begin{aligned}
\frac{\partial \hat{C}_{if}}{\partial \hat{t}} &= \alpha\rho(\hat{C}_{ef} - \hat{C}_{if}) - k_1T_0\tilde{t}\left(\hat{B} - \hat{C}_{is}\right)\hat{C}_{if} + \frac{k_2T_0}{\bar{K}}\hat{C}_{is} - k_3\tilde{t}\hat{C}_{if} + k_4\tilde{t}\hat{C}_{ins}\,,\\
\frac{\partial \hat{C}_{is}}{\partial \hat{t}} &= k_1\bar{K}\tilde{t}(\hat{B} - \hat{C}_{is})\hat{C}_{if} - k_2\tilde{t}\hat{C}_{is}\,,\\
\frac{\partial \hat{C}_{ins}}{\partial \hat{t}} &= k_3\tilde{t}\hat{C}_{if} - k_4\tilde{t}\hat{C}_{ins})\,,\\
\frac{\partial \hat{C}_{ef}}{\partial \hat{t}} &= \frac{D\tilde{t}}{L^2}\frac{\partial^2\hat{C}_{ef}}{\partial\hat{z}^2} + \alpha(1-\rho_0\hat{\rho})(\hat{C}_{if} - \hat{C}_{ef}) - k_5\tilde{t}\hat{C}_{ef} + k_6\tilde{t}\hat{C}_{ens}\,,\\
\frac{\partial \hat{C}_{ens}}{\partial \hat{t}} &= k_5\tilde{t}\hat{C}_{ef} - k_6\tilde{t}\hat{C}_{ens}\\
\frac{\partial \hat{T}}{\partial \hat{t}} &= \frac{a_1\tilde{t}}{T_0} + a_2\tilde{t}\hat{C}_{is} - a_3\tilde{t}(\hat{T} - \hat{B})\,,\\
\frac{\partial \hat{B}}{\partial \hat{t}} &= \left(\beta_1\tilde{t} + \beta_2\tilde{t}T_0\hat{C}_{is}\right)(\hat{T} - \hat{B}) - 2\beta_1\tilde{t}\hat{B}\,,
\end{aligned} \tag{24}$$

and for $\delta_1 < \hat{z} < \delta_2$ we have

$$\begin{aligned}
\frac{\partial \hat{C}_{ef}}{\partial \hat{t}} &= \frac{D\tilde{t}}{L^2}\frac{\partial^2\hat{C}_{ef}}{\partial\hat{z}^2} - k_5\tilde{t}\hat{C}_{ef} + k_6\tilde{t}\hat{C}_{ens}\,,\\
\frac{\partial \hat{C}_{ens}}{\partial \hat{t}} &= k_5\tilde{t}\hat{C}_{ef} - k_6\tilde{t}\hat{C}_{ens}
\end{aligned} \tag{25}$$

The initial conditions in the cellular domain $(0 < \hat{z} < \delta_1)$ are

$$\hat{C}_{if}(\hat{z},0) = \hat{C}_{is}(\hat{z},0) = \hat{C}_{ins}(\hat{z},0) = 0\,,\ \hat{C}_{ef}(\hat{z},0) = \hat{C}_0\,,$$
$$\hat{C}_{ens}(\hat{z},0) = 0\,,\ \hat{T}(\hat{z},0) = 1\,,\ \hat{B}(\hat{z},0) = \tilde{B}\,,$$

The initial conditions in the extracellular domain ($\delta_1 < \hat{z} < \delta_2$) are

$$\hat{C}_{ef}(\hat{z},0) = C_0\,,\ \hat{C}_{ens}(\hat{z},0) = 0\,.$$

The system is closed with the zero-flux boundary conditions:

$$\left.\frac{\partial \hat{C}_{ef}}{\partial \hat{z}}\right|_{(0,\hat{t})} = 0, \quad \left.\frac{\partial \hat{C}_{es}}{\partial \hat{z}}\right|_{(0,\hat{t})} = 0, \quad \left.\frac{\partial \hat{C}_{ef}}{\partial \hat{z}}\right|_{(\delta_2,\hat{t})} = 0, \quad \left.\frac{\partial \hat{C}_{es}}{\partial \hat{z}}\right|_{(\delta_2,\hat{t})} = 0\,. \tag{26}$$

Now introduce the dimensionless parameters

$$\tilde{\lambda_1} = \alpha\rho\tilde{t}, \quad \lambda_2 = \frac{k_1\bar{K}}{k_2}, \quad \lambda_3 = \frac{k_3}{k_4}, \quad \lambda_4 = k_5\tilde{t}, \quad \lambda_5 = k_6\tilde{t},$$
$$\lambda_6 = \frac{a_1\tilde{t}}{T_0}, \quad \lambda_7 = a_3\tilde{t}, \quad \lambda_8 = \beta_1\tilde{t}, \quad \lambda_9 = \beta_2 T_0\tilde{t}, \quad \bar{D} = \frac{D\tilde{t}}{L^2}\,. \tag{27}$$

Dropping hats, taking $\tilde{t} = 1$, and applying the simplifications (vii)–(xii), stated in Section 2.2.1, specifically the quasi-steady state assumptions on $\hat{C}_{is}$ and $\hat{C}_{ins}$; and substituting the constants λ_i and $\bar{D}$ as defined above, we obtain model (4),(5).

A.3 Volume variation protocol

In the cases of the experiment where the volume of the culture medium was varied (see Figures 4) (d) and 5 (d) for the corresponding data), the height of the fluid in the dish would correspondingly change. The height of the fluid in each case was approximated by the following calculation

$$h_i = \frac{V_{medium,i}}{\pi R^2}\,.$$

The volumes of medium used are $V_{medium,1} = 1ml$, $V_{medium,2} = 2ml$ and $V_{medium,3} = 10ml$, which are equivalently $1\,, 2$ and $10cm^3$. The radius of the dish is $R = 1.75cm$, hence in the case of 1 ml of of culture medium used, we have that

$$h_1 = \frac{1}{\pi \times 1.75^2} = \frac{1}{9.62} \approx 0.1\,,$$
$$h_2 = \frac{2}{\pi \times 1.75^2} = \frac{2}{9.62} \approx 0.2\,,$$
$$h_3 = \frac{10}{\pi \times 1.75^2} = \frac{10}{9.62} \approx 1,.$$

The values for the different fluid heights are summarised in Table 1.

Volume of Medium (ml)	Fluid Height (cm)
1	$h_1 = 0.1$
2	$h_2 = 0.2$
10	$h_3 = Z_0 = 1$

Table 1: Table of calculated fluid heights used in the various experiments.

A.4 Model Parameters

Total number of iterations	Ψ	2500
Burn in period	Ψ_b	200

Table 2: Number of iterations and burn in duration for the Gibbs sampler

Parameter	Prior LB	Value	Prior UB	Value
λ_1 ($\tilde{\lambda}_1$)	a_{l1}	0	b_{u1}	10000
λ_2	a_{l2}	10	b_{u2}	500
λ_3	a_{l3}	0	b_{u3}	100
λ_4	a_{l4}	0	b_{u4}	400
λ_5	a_{l5}	0	b_{u5}	1
λ_9	a_{l6}	0	b_{u6}	15

Table 3: Upper and lower bounds on the uniform priors used when sampling the parameters.

Fitted Parameter	Grouping	ODE value	PDE value
λ_1	$\frac{\alpha \tilde{t}}{V_{onecell}}$	361.3	
$\tilde{\lambda}_1$	$\alpha \rho \tilde{t}$		1227
λ_2	$\frac{k_1 \bar{K}}{k_2}$	149	152
λ_3	$\frac{k_3}{k_4}$	72.4	72.4
λ_4	$k_5 \tilde{t}$	0.806	0.806
λ_5	$k_6 \tilde{t}$	0.085	0.0791
λ_9	$\beta_2 T_0 \tilde{t}$	11.59	11.67
Fixed Parameter	Grouping		
λ_6	$\frac{a_1 \tilde{t}}{T_0}$	62.3	62.3
λ_7	$a_3 \tilde{t}$	21.52	21.52
λ_8	$\beta_1 \tilde{t}$	21.6	21.6
$\tilde{B}$	$\frac{B_0}{T_0}$	$\frac{1}{3}$	$\frac{1}{3}$
$V_{onecell}$	mm^3	2.54×10^{-6}	
V_{medium}	mm^3	$1\,, 2\,, 10 \times 10^3$	
N_0		0.7×10^6	
$\bar{D}$	$\frac{D\tilde{t}}{Z_0^2}$		0.015
ρ	$\frac{N_0 V_{onecell}}{\pi R^2 d}$		0.013
δ_1	$\frac{d}{Z_0}$		10^{-4}
δ_2	$\frac{h_i}{Z_0}$		$0.1\,, 0.2\,, 1$

Table 4: Values of all parameters used. 'ODE value' column corresponds to values used or fitted in Sections 3.1 with results plotted in Figure 4. 'PDE value' column corresponds to values used or fitted in Section 3.2, with results plotted in Figure 5.

Parameter	Units	ODE inferred value	PDE inferred value	
k_1	$nM^{-1}h^{-1}$			
k_2	h^{-1}	$18.72k_1$	$17.8k_1$	
k_3	h^{-1}	$72.4k_4$	$79.1k_4$	
k_4	h^{-1}			
k_5	nMh^{-1}	72	72	
k_6	h^{-1}	0.11	0.11	
α	μLh^{-1}	2.32×10^3	8.53×10^3	
β_2	h^{-1}	11.59	11.67	
Fixed Parameter	Units	ODE value	PDE value	Reference
$a_1 = a_3(T_0 - B_0)$	μMh^{-1}	0.1869	0.1869	
a_3	h^{-1}	0.0163	0.0163	
β_1	h^{-1}	21.6	21.6	[32]
$\beta_3 = 2\beta_1$	nM	43.2	43.2	
D	cm^2h^{-1}		0.15	[28]
T_0	μM	18.9	18.9	[24]
B_0	μM	6.3	6.3	[24]
$V_{onecell}$	μm^3	2.54×10^3	2.54×10^3	
d	μm		10	

Table 5: Units of all model parameters, and, where applicable, their inferred values from Table 4. 'ODE inferred value' column corresponds to values fitted in Section 3.1 with results plotted in Figure 4. 'PDE inferred value' column corresponds to values fitted in Section 3.2, with results plotted in Figure 5.

B Parameter fitting and identification

B.1 Fit to the medium data

Having observed that the total paclitaxel concentration in the medium without cells is a decreasing function of time (see Figure 3 (b)), we assumed that paclitaxel can reversibly transfer to a nondetectable pool, with the concentration of paclitaxel in this pool given by $C_{ens}(t)$. Since there are no cells present, the only nonzero concentrations are the extracellular paclitaxel concentrations. Hence, a reduced version of equations (1), (2) is used to describe the experimental setup without cells presented in Figure 3 (b). This is given by the following system of equations

$$\begin{aligned} \frac{dC_{ef}}{dt} &= -\lambda_4 C_{ef} + \lambda_5 C_{ens}\,, \\ \frac{dC_{ens}}{dt} &= \lambda_4 C_{ef} - \lambda_5 C_{ens}\,, \end{aligned} \tag{28}$$

with the initial conditions

$$C_{ef} = C_0\,, \quad C_{ens} = 0\,.$$

Figure 6: Histograms of the accepted sampled values from the uniform priors for: (a) λ_4 and (b) λ_5. The counts have been normalized to a density, with the density functions of the fitted Gaussian distributions plotted in red.

To determine optimal values for the parameters λ_4 and λ_5 (see Table 3), we applied Bayesian inference to the data in Figure 3 (b), using the Gibbs sampler to generate an estimate of the posteriror distributions of λ_4 and λ_5 as described in Methods 2.4.

To check that the Gibbs sampler had converged to a unique maximum of the likelihood 13 for the parameters λ_4 and λ_5 fitted in Section 3.1, the histograms of the accepted values of both of their parameters are plotted in Figure 6. It is clear that the distributions of the sampled values for both parameters are unimodal.

B.2 Fit of the full model

Figure 7 presents pairwise scatter plots of the sampled values of the fitted parameters at each iteration of the algorithm as well as histograms of the fitted parameters.

C Comparing the ODE and PDE models

To determine whether both the ODE and PDE models converged to the same steady state. Both equations (1), (2) and (4) – (6) were simulated over 50 hours for cells in a volume of 10ml of medium with an initial concentration of 200nM (this is the maximum concentration and volume used in the experiments). At 20 hours there is still some difference between the total concentrations (see Figure 8). Beyond 30 hours both systems have reached equilibrium, with the stationary value of the intracellular concentration the same up to numerical error.

Figure 7: (b) – (d), (f), (g) and (i) are pairwise scatter plots of the sampled parameter values at each iteration of the Gibbs sampler. Black dotted lines indicate the sample median for each of the parameters. On the diagonal (a), (e), (h), (j) are histograms of the accepted sample values of the parameters. The red curves correspond to the density functions of the Gaussian distributions fitted to the sample distribution for each parameter.

To determine if there was a timescale over which diffusion had a significant effect on paclitaxel uptake when 1 ml of culture medium was used (corresponding to the length of the spatial domain being 1 mm), both models, with the parameter values as in Table 4, were simulated over 2 hours with an initial concentration of 20 nM. Whilst the simulated concentration profiles are similar, it is clear that the concentration given by the PDE system is slightly below the one given by the ODE system until after approximately 2 hours (see Figure 8).

Figure 8: Comparison of time series plots of the total and averaged over spacial domain total intracellular concentration $C(t)$ for the ODE and PDE models over a time series. (a) Plot of the total intracellular concentration profiles for both the ODE and PDE models when simulated with an initial concentration of 200 nM for 50 hours in a medium of 10 ml. (b) Plot of the total intracellular concentration profiles for both the ODE and PDE models when simulated with an initial concentration of 20 nM for 2 hours in a medium of 1 ml.

Figure 9 illustrates simulation results for the average intracellular concentrations for both models when simulated for half an hour, 2 hours, 4 hours and 20 hours and for different medium volumes. Both the PDE and ODE models have nearly identical concentrations at the lowest volumes for all the time points considered. At the higher volumes, the PDE is consistently above the ODE.

Figure 9: Plots of the total and averaged total intracellular concentration $C(t)$ at different time points for numerical simulations of the ODE and PDE models across a variety of medium volumes - solid curves for the ODE model and dashed curves for the PDE model. Colours correspond to different volumes of the medium: cyan - 0.1ml; black - 0.5 ml; green - 1ml; red - 5ml; magenta - 10 ml. Total intracellular concentrations are plotted for the following times: (a) after 2 hours, (b) after 20 hours.

D Alternative models for paclitaxel in medium

D.1 Linear degradation of free paclitaxel

Here we consider an alternative hypothesis that degradation causes the loss of paclitaxel from the medium, instead of binding to the containers. This is included as a linear rate of $k_7 C_{ef}$ in the equations for extracellular paclitaxel:

$$\frac{dC_{ef}}{dt} = -k_7 C_{ef}\,, \tag{29}$$

When nondimensionalized we obtain

$$\frac{dC_{ef}}{dt} = -\lambda_{10} C_{ef}\,, \tag{30}$$

In Figure 10, we see that linear degradation can explain the loss of total extracellular paclitaxel in the data presented. However, the numerical solution with the best fit value of λ_{10} does not maximise the likelihood (13) as well as the fit of equations (1), (2). This is apparent when comparing Figure 10 with Figure 3.

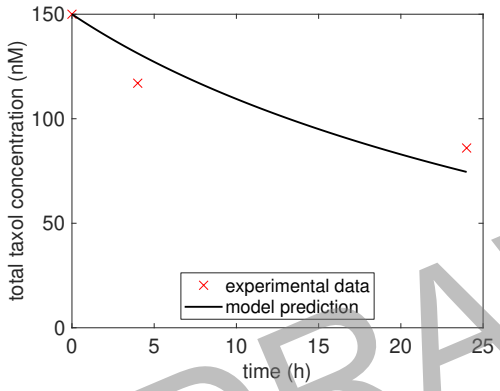

Figure 10: Total extracellular paclitaxel concentration is plotted against time. Black line - rescaled numerical solution of C_{ef} from system (30). Red crosses - measured free paclitaxel concentration in extracellular media.

It's clear that the equations (1), (2), with C_{ens} removed and the equation for C_{ef} replaced by (30) captures the same behaviour with respect to the total intracellular concentration of paclitaxel amassed in the cells, as well as the timescale for the uptake and release of paclitaxel after a washout. This apparent when we compare Figures 11 (a) – (c) with Figures 4 (a) – (c). Furthermore, whilst this model captures the behaviour of paclitaxel observed in the experiments when the volume of the medium is 2ml, simulations of the model for different volumes of the medium across a range of initial concentrations demonstrates that equations (1), (2), with linear degradation of paclitaxel in the medium fail to predict the results.

Figure 11: Plot of the full set of experimental data with the cells included, with the best fit parameters for the degradation model (30). (a) Total intracellular paclitaxel concentration, $C(t)$, is plotted against time. Control media (circles - experimental data, solid line - model solution). (b) Total intracellular paclitaxel concentration, $C(t)$, is plotted against initial paclitaxel concentration, C_0, after a two hour paclitaxel incubation (crosses - experimental data, solid black line - model solution) followed by eight hours in control media (red and blue circles-experimental data, dotted black line - model solution). (c) Total intracellular paclitaxel concentration, $C(t)$, is plotted against time after 2 hours of incubation of cells in 100nM of paclitaxel (red markers - data, red curve - model with fitted parameters). (d) Total intracellular paclitaxel concentration after a two hour incubation, $C(2)$ is plotted against initial concentration, C_0, for different media volumes (1 ml - red, 2 ml - blue and 10 ml -black) (lines - model solutions, crosses - experimental data). The model was solved using the Method defined in Section 2.3.

D.2 Binding of paclitaxel to the culture medium

In order to test whether the model results are robust to the inclusion of paclitaxel binding with the culture medium, which was observed in previous studies [25, 33], we modified equations (1), (2) to account for an additional compartment of saturable bound extracellular paclitaxel. We let $C_{es}(t)$ be the concentration of paclitaxel that is bound to the culture medium after t hours, which we assume to follow Michaelis-Menten like kinetics. We obtain the following system of equations after nondimensionalizing and simplifying:

$$\begin{aligned}
\frac{dC_{if}}{dt} &= \lambda_1(C_{ef} - C_{if})\,,\\
C_{is} &= \frac{BC_{if}}{\frac{1}{\lambda_2} + C_{if}}\,,\\
C_{ins} &= \lambda_3 C_{if}\,,\\
\frac{dC_{ef}}{dt} &= \lambda_1 N_0 \frac{V_{onecell}}{V_{medium}}(C_{if} - C_{ef}) - \lambda_4 C_{ef} + \lambda_5 C_{ens}\\
&\quad + \lambda_{10}\left(C_{es} - \frac{C_{ef}}{1 + C_{ef}}\right),\\
\frac{dC_{ens}}{dt} &= \lambda_4 C_{ef} - \lambda_5 C_{ens}\,,\\
\frac{dC_{es}}{dt} &= \lambda_{11}\left(\frac{C_{ef}}{1 + C_{ef}} - C_{es}\right)\,,\\
\frac{dT}{dt} &= \lambda_6 - \lambda_7(T - B)\,,\\
\frac{dB}{dt} &= (\lambda_8 + \lambda_9 C_{is})\,(T - B) - 2\lambda_8 B\,,
\end{aligned} \tag{31}$$

with initial conditions are given by

$$C_{if}(0) = C_{is}(0) = C_{ins}(0) = 0, \quad C_{ef}(0) = C_0, \quad C_{es}(0) = 0,$$
$$C_{ens}(0) = 0, \quad T(0) = \frac{T_0}{B_0}\,,\ B(0) = 1.$$

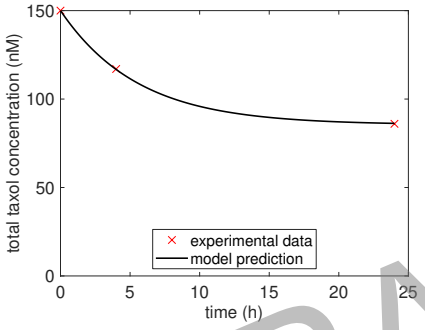

Figure 12: Total extracellular paclitaxel concentration is plotted against time. Black line - rescaled numerical solution of $C_{ef} + C_{es}$ from system (28). Red crosses - measured free paclitaxel concentration in extracellular media.

It can be seen in Figures 13 (a) – (d) that the numerical simulations of model (31) captures the same behaviour with respect to the total intracellular concentration of paclitaxel amassed in the cells, as well as the timescale for the uptake and release of paclitaxel after a washout, as seen in the Results section 3.1.

Figure 13: Full experimental data of paclitaxel with cells, with the model with medium binding fitted to it. (a) Total intracellular paclitaxel concentration, $C(t)$, is plotted against time. Control media (circles - experimental data, solid line - model solution). (b) Total intracellular paclitaxel concentration, $C(t)$, is plotted against initial paclitaxel concentration, C_0, after a two hour paclitaxel incubation (crosses - experimental data, solid black line - model solution) followed by eight hours in control media (red and blue circles- experimental data, dotted black line - model solution). (c) Total intracellular paclitaxel concentration, $C(t)$, is plotted against time after 2 hours of incubation of cells in 100nM of paclitaxel (red markers - data, red curve - model with fitted parameters). (d) Total intracellular paclitaxel concentration after a two hour incubation, $C(2)$ is plotted against initial concentration, C_0, for different media volumes (1 ml - red, 2 ml - blue and 10 ml -black) (lines - model solutions, crosses - experimental data). The model was solved using the Method defined in Section 2.3.

References

[1] Hanahan D and Weinberg RA. Hallmarks of cancer: the next generation. *Cell*, 144:646 – 674, 2011.

[2] Smittenaar CR et al. Cancer incidence and mortality projections in the uk until 2035. *British Journal of Cancer*, 115(9):1147–1155, 2016.

[3] Lyman GH. Chemotherapy dose intensity and quality cancer care. *Oncology (Williston Park*, 20(14 Suppl 9):16–25, 2006.

[4] Wani MC et al. Plant antitumor agents. vi. the isolation and structure of taxol, a novel antileukemic and antitumor agent from taxus brevifolia. *Journal of the American CHemistry Society*, 93(9):2325–7, 1971.

[5] BA Chabner and TG Roberts. Timeline: chemotherapy and the war on cancer. *Nature Reviews Cancer; 5(1)*, 2005.

[6] J Shi and TJ Mitchison. Cell death response to anti-mitotic drug treatment in cell culture, mouse tumor model and the clinic. *Endocrine Related Cancer; 83-96*, 2017.

[7] Schiff PB and Horwitz SB. Taxol stabilizes microtubules in mouse fibroblast cells. *Proceedings of the National Academy of Science U.S.A.*, 77(3):1561–5, 1980.

[8] Weaver et al. How taxol/paclitaxel kills cancer cells. *Molecular Biology of the Cell*, 2014.

[9] Zasadil LM et al. Cytotoxicity of paclitaxel in breast cancer is due to chromosome missegregation on multipolar spindles. *Science Translational Medicine*, 26(6):229, 2014.

[10] Sparano J et al. Weekly paclitaxel in the adjuvant treatment of breast cancer. *New England Journal of Medicine*, 2008.

[11] Bonomi P. Review of paclitaxel/carboplatin in advanced non-small cell lung cancer. *Seminars in Oncology*, 26(1 Suppl 2):55–59, 1999.

[12] Coleman Obasaju MD and Gary R. Hudes MD. Paclitaxel and docetaxel in prostate cancer. *Hematology/Oncology Clinics of North America*, 2001.

[13] Kapman NC et al. Paclitaxel and its evolving role in the management of ovarian cancer. *BioMed Research International*, vol. 2015, 2015.

[14] Spencer CM and Faulds D. Review of paclitaxel/carboplatin in advanced non-small cell lung cancer. *Drugs*, 48(5):794–847, 1994.

[15] Scripture CD et al. Peripheral neuropathy induced by paclitaxel: Recent insights and future perspectives. *Current Neuropharmacology*, 4:165 – 172, 2006.

[16] Tischer J and Gergely F. Anti-mitotic therapies in cancer. *The journal of Cell Biology*, 218(1):10–11, 2019.

[17] Olziersky AM and Labdi-Galy SI. Clinical development of anti-mitotic drugs in cancer. In *Advances in experimental medicine and biology*, pages 125–152. Springer, 2017.

[18] Sackett DL Komlodi-Pasztor E and Fojo AT. Inhibitors targeting mitosis: tales of how great drugs against a promising target were brought down by a flawed rationale. *Clinical Cancer Research*, 18(1):51–63, 2012.

[19] Perez EA. Paclitaxel in breast cancer. *The oncologist*, 3(6):373–389, 1998.

[20] Gianni L Kearns CM and Egorin MJ. Paclitaxel pharmacokinetics and pharmacodynamics. *Seminars in oncology*, 22(3 Suppl 6):16–23, 1995.

[21] Mori T et al. Retention of paclitaxel in cancer cells for 1 week in vivo and in vitro. *Cancer Chemotherapy and Pharmacology*, 58(5):665 – 672, 2006.

[22] Parness J Manfredi JJ and Horwitz SB. Taxol binds to cellular microtubules. *Journal of Cell Biology*, 94:688 – 696, 1982.

[23] Lowe J et al. Refined structure of α , β -tubulin at 3.5 p resolution. *Journal of Molecular Biology*, 313:1045 – 1057, 2001.

[24] Thrower D Jordan MA, Toso RJ and Wilson L. Mechanism of mitotic block and inhibition of cell proliferation by taxol at low concentrations. *Cancer Research*, 1993.

[25] Kuh et al. Computational model of intracellular pharmacokinetics of paclitaxel. *The Journal of Pharmacology and Experimental Therapeutics*, 2000.

[26] Matsson P Mateus A and Artursson P et al. Rapid measurement of intracellular unbound drug concentrations. *Molecular Pharmaceutics*, 10:24678–2478, 2013.

[27] MATLAB. *version 9.5.0.1 (R2018b)*. Natick, Massachusetts, 2018.

[28] Cremasco MA and Wang LNH. Estimation of partition, free and specific diffusion coefficients of paclitaxel and taxanes in a fixed bed by moment analysis: experimental, modeling and simulation studies. *Acta Scientarium Tewchnology*, 34(1), 2012.

[29] E. et al. Komlodi-Pasztor. Mitosisis not a key target of microtubule agents in patient tumours. *National Review of Clinical Oncology 8; 244-250*, 2011.

[30] Mitchison T. The proliferation rate paradox in antimitotic chemotherapy. *Mol Biol Cell*, 2012.

[31] Mitchison TJ et al. Is inflammatory micronucleation the key to a successful anti-mitotic cancer drug? *Open Biology*, 7(11), 2017.

[32] Erickson HP and O'Brien ET. Microtubule dyamic instability and gtp hydrolysis. *Annual Review of Biophysics and Biomolecular Structure*, 1992.

[33] Song et al. Binding of taxol to plastic and glass containers and protein under in vitro conditions. *Journal of Pharmaceutical Sciences*, 1996.